Title

MRI - Based Measures of Metabolic Health in the Assessment of Patients with Chronic Inflammatory States

Author

Anbu Rajan, Siddharthasiva

Publication Date

2024

Peer reviewed|Thesis/dissertation

MRI - Based Measures of Metabolic Health in the Assessment of Patients with Chronic Inflammatory States

by
Siddharthasiva Anbu Rajan

THESIS
Submitted in partial satisfaction of the requirements for degree of
MASTER OF SCIENCE

in

Biomedical Imaging

in the

GRADUATE DIVISION
of the
UNIVERSITY OF CALIFORNIA, SAN FRANCISCO

Approved:

DocuSigned by:
Susan Noworolski
070ED2AA0DC3441...

Susan Noworolski
Chair

DocuSigned by:
Diana Alba
[illegible]

Diana Alba

DocuSigned by:
Jing Liu
[illegible]429...

Jing Liu

DocuSigned by:
Michael Ohliger
EB514B0EC25145F...

Michael Ohliger

Committee Members

ACKNOWLEDGEMENTS

I would like to acknowledge and thank Dr. Susan Noworolski and Dr. Matthew Gibbons for their help, guidance, and constant support during the entire process of completing this thesis project. I would also like to thank Edgar Castellanos for his help and the training guides he wrote, which helped me ease into my role as a part of the Abdominopelvic Imaging Laboratory.

My sincere thanks to my panel members, Dr. Diana Alba, Dr. Jing Liu, and Dr. Michael Ohliger, for their feedback, which pushed me to think deeper and answer more questions than I initially set out to answer.

This work was possible because "I was standing on the shoulders of giants." My family, teachers, mentors, friends, and peers have supported me towards completing the MS in Biomedical Imaging Program at UCSF. I would like to thank these "giants" for helping me get this far and dedicate this manuscript to them.

MRI-BASED MEASURES OF METABOLIC HEALTH IN THE ASSESSMENT OF PATIENTS WITH CHRONIC INFLAMMATORY STATES

SIDDHARTHASIVA ANBU RAJAN

ABSTRACT

Disease conditions like obstructive sleep apnea (OSA) and human immunodeficiency virus (HIV) infections are characterized by chronic low-grade inflammation, leading to poor metabolic health. This work is focused on comparing MR-based fat measures to indicators of worse metabolic health, namely OSA severity and hydroxyproline, a biomarker of subcutaneous fat (SAT) fibrosis. The study also explored the utility of novel MRI methods of diffusion-weighted imaging of fat and T1 mapping to detect fibrosis in the SAT. There were 33 participants with OSA and 58 participants with or without HIV infection who had hydroxyproline measured via SAT biopsy, 13 of whom had the novel MRI measures of fibrosis. The liver, visceral, and SAT volumes were segmented using artificial intelligence-based methods, and the pancreas was manually drawn on proton density fat fraction (PDFF) images. Apparent diffusion coefficient (ADC) and T1 were measured in regions of interest drawn in the SAT. Liver fat fraction, liver fat content, and pancreatic fat fraction were higher with increased severities of sleep apnea, $p \leq 0.01$. Furthermore, liver fat fraction, pancreatic fat fraction, and visceral fat volume were higher in subjects with high hydroxyproline levels on biopsy, $p \leq 0.03$. The ADC of SAT at b-values of 3×10^{-3} s/mm^2 were negatively correlated with hydroxyproline levels. It can be concluded that more severe OSA and higher hydroxyproline were associated with worse metabolic health. The role of diffusion-weighted imaging of fat with high b-values to detect SAT fibrosis is also encouraging and opens up avenues for future research.

TABLE OF CONTENTS

LIST OF FIGURES

LIST OF TABLES

LIST OF ABBREVIATIONS

ADC	-	Apparent Diffusion Coefficient
AHI	-	Apnea-Hypopnea Index
AUC	-	Area Under the Curve
BMI	-	Body Mass Index
CNN	-	Convolutional Neural Network
DWI	-	Diffusion-Weighted Imaging
DXA	-	Dual-Energy X-ray Absorptiometry
FF	-	Fat Fraction
FOV	-	Field of View
HIV	-	Human Immunodeficiency Virus
HOMA-IR	-	Homeostatic Model Assessment of Insulin Resistance
IDEAL-IQ	-	Iterative Decomposition of Water and Fat with Echo Asymmetry and Least-squares Estimation and Quantification
IDEO	-	Inflammation, Diabetes, Ethnicity, and Obesity
IRSA	-	Insulin Resistance and Sleep Apnea
MASLD	-	Metabolic Dysfunction-Associated Steatotic Liver Disease
MRI	-	Magnetic Resonance Imaging
NCD	-	Non-Communicable Disease
NEX	-	Number of Excitations
OSA	-	Obstructive Sleep Apnea
PDFF	-	Proton Density Fat Fraction

ROC	-	Receiver Operating Characteristic
ROI	-	Region of Interest
SAT	-	Subcutaneous Adipose Tissue
TE	-	Echo Time
TI	-	Inversion Time
TR	-	Repetition Time
VAT	-	Visceral Adipose Tissue
WHO	-	World Health Organization

CHAPTER 1 – INTRODUCTION:

Non-communicable diseases (NCDs) are a leading cause of morbidity and mortality across the world. Initially a set of diseases and conditions prevalent in developed nations, global industrialization and rapid economic development in the past decade have helped NCDs evolve into a global pandemic. This change has increased with the prevalence of modifiable risk factors such as physical inactivity and unhealthy diets. According to the World Health Organization (WHO), NCDs are responsible for 41 million deaths worldwide.[1] Metabolic syndrome, defined by a constellation of conditions associated with dysregulation of glucose and lipid metabolism, acts as a common feature of non-communicable diseases like Type II diabetes mellitus and cardiovascular diseases. The key features of metabolic syndrome include central obesity, dyslipidemia, hyperglycemia, and hypertension.[2]

Chronic inflammatory conditions are also closely associated with the development and progression of metabolic syndrome and insulin resistance. Studies have shown that pro-inflammatory cytokines play a role in the propagation of insulin resistance and poor metabolic outcomes.[3][4] Obstructive sleep apnea and chronic HIV infection are two such conditions that, through different mechanisms, are linked to poor metabolic health outcomes. Obstructive sleep apnea (OSA) is a sleep-associated breathing disorder with intermittent episodes of decreased depth of breathing (hypopnea) and cessations of breathing (apnea). According to a 2023 meta-analysis, OSA has a global prevalence of 54%.[5] The intermittent hypoxic stress that is caused by the episodes of hypopneas and apneas is postulated to cause a chronic inflammatory state that can drive abnormal metabolism and storage of fat in the body.[6] HIV infection is also associated with

disordered storage of fat.[7] Patients with chronic HIV infection states are known to present with regional increases and losses of fat. The immune activation seen in HIV infection can contribute to inflammation, which can derange fat storage. Another aspect of this story is the concept of subcutaneous adipose tissue fibrosis. Changes in the metabolism (which may or may not be associated with obesity) of adipose tissue trigger inflammation, which in turn triggers a maladaptive repair response in the tissue and abnormal fibrotic extracellular matrix expansion.[8] This obesity and fibrosis, in combination, contribute to insulin resistance and ectopic fat accumulation in the visceral compartments of the abdomen.

1.1 – Significance:

Clinical measures of metabolic syndrome, such as body mass index (BMI) and waist circumference, do not account for the variability in fat depots in the subcutaneous adipose tissue (SAT) and visceral adipose tissue (VAT).[2] Visceral adipose tissue is generally known to be more metabolically active than its subcutaneous counterpart. They are more insulin resistant and have a higher potential to generate free fatty acids that can deposit in visceral organs like the liver and pancreas.[9] Obesity and metabolic syndrome are also associated with higher levels of fat deposition in the liver and pancreas.[10] [11] In fact, there is increasing adoption of the term metabolic dysfunction associated steatotic liver disease (MASLD) to describe this fat accumulation in the liver that is not associated with alcohol use.[12] Steatosis in the liver can be diagnosed using liver biopsies, but this suffers the disadvantages of being invasive, subjective, prone to under-sampling, and graded into broad categories. Taking all these into consideration, there exists an unmet need to come up with an image-based approach to diagnose and quantify the effect of metabolic

syndrome in patients with chronic inflammatory conditions, particularly to determine the impact of interventions.

MRI proton density fat fraction (PDFF) imaging is a non-invasive method to quantify the fat concentration of a tissue of interest. It uses chemical-shift-based separation of signal from fat and water to quantify the fraction of fat in the tissue. According to the conventional technique described by WT Dixon[13], magnitude images acquired at different echo times (TEs), owing to the different resonant frequencies of fat and water, would result in fat and water being in-phase or out-of-phase to each other. In-phase images would be a combination of signals from water and fat, whereas an out-of-phase image comprises signals from water minus fat. These two images can be added or subtracted to get water-only and fat-only images.[14] The disadvantage of this method is that since only magnitude images are used, tissue that is almost pure fat would have similar signal on in-phase and out-of-phase images. Hence, water-only images would have falsely elevated signal, and fat-only images would have falsely diminished signal intensity. Current conventional methods like the IDEAL method (iterative decomposition of water and fat with echo asymmetry and least square estimation) use multiple echoes and mathematical modeling with maximum likelihood estimation to get more accurate fat fraction estimates.[14] While various studies have established MRI PDFF as a standardized method to estimate liver fat content[15] [16], pancreatic fat estimation and adipose tissue fat estimation are also gaining traction.[17] [18]

There is also potential for exploring the utility of novel MRI techniques like fat fraction mapping, diffusion-weighted imaging (DWI) of fat with high b-values, and T1-mapping in detecting and possibly quantifying fibrosis of fat. Exploratory analysis with a limited

sample size can help gain insight into optimizing and improving the image acquisition and reconstruction pipeline to quantify fibrosis better.

1.2 – Approach:

This project was an observational prospective cohort study of 2 groups of participants with different sets of independent variables. The first group of independent variables were the measures of severity of OSA. They were compared against a set of MRI metrics that could help understand and quantify fat distribution in the abdomen. The second set of variables in the second cohort is hydroxyproline levels from abdominal fat biopsy. This is a measure of fibrosis in the fat. This is compared against the same MRI metrics.

Further analysis across both cohorts also involves comparing the MRI metrics against biochemical tests like glucose, insulin, lipid profiles, and insulin resistance scores. This manuscript is divided into sections based on the different cohorts and objectives being investigated. Chapter 2 deals with the overall goals and hypotheses of the project. Chapter 3 will outline the general study design and MRI techniques used. Chapter 4 will relate the study group, processing pipeline, and analysis and present the results of the OSA cohort. Chapter 5 will do the same for the IDEO cohort. Chapter 6 will be about the exploratory investigations of the study. Chapter 7 will conclude the manuscript with a discussion summarizing the entire project.

CHAPTER 2 – OBJECTIVES:

The objectives of this study were the following:

1. To determine if ectopic fat measures are higher across different severity categories in obstructive sleep apnea (OSA).
2. To determine if subjects with higher levels of hydroxyproline on abdominal fat biopsy correlate with lower levels of subcutaneous adipose tissue (SAT) and higher levels of ectopic fat measures compared to subjects with low hydroxyproline.
3. To determine if these fat measures correlated with poor metabolic health in the IDEO and OSA cohorts.
4. To determine if novel MRI techniques such as diffusion-weighted imaging (DWI) of fat and T1 mapping can identify fibrosis in fat and if the measures correlate with the severity of fibrosis measured by hydroxyproline levels on subcutaneous biopsy.

Based on existing literature about metabolic dysfunction and the use of imaging biomarkers to quantify fat and fibrosis, we hypothesized the following:

1. Patients with severe OSA (AHI>30) will have higher levels of fat in the liver, pancreas, and visceral compartment when compared to patients with milder forms of the disease.
2. Fat fraction of subcutaneous tissue will be lower, and ectopic fat volumes will be higher in patients with high hydroxyproline on subcutaneous biopsy.
3. Measures of ectopic fat will correlate with poor metabolic health in both cohorts.
4. Fibrosis of fat can be measured with DWI and T1 mapping.

CHAPTER 3 – METHODS:

3.1 – Study Design:

The study had a prospective observational study design (Figure 3.1). The participants from both cohorts were continuously recruited, and metabolic analysis and MR imaging were done. A specific set of metrics from MR imaging was selected. These variables include VAT and SAT volume and fat fraction at L3-L4 intervertebral level, liver fat fraction, liver fat content (product of liver fat fraction and segmented liver volume), and pancreatic fat fraction. These metrics are compared with hydroxyproline levels as a continuous variable and as categories for the IDEO cohort. For the OSA cohort, the MRI metrics were compared against the apnea-hypopnea index (AHI) as a continuous score and as categories (mild, moderate, and severe). Statistical analysis was then done between these variables for both groups. The fourth objective of the study was investigated using a small sample of subjects from the IDEO cohort. The SAT fat fraction, ADC values, and T1 values were compared on this subset of participants and compared against hydroxyproline levels.

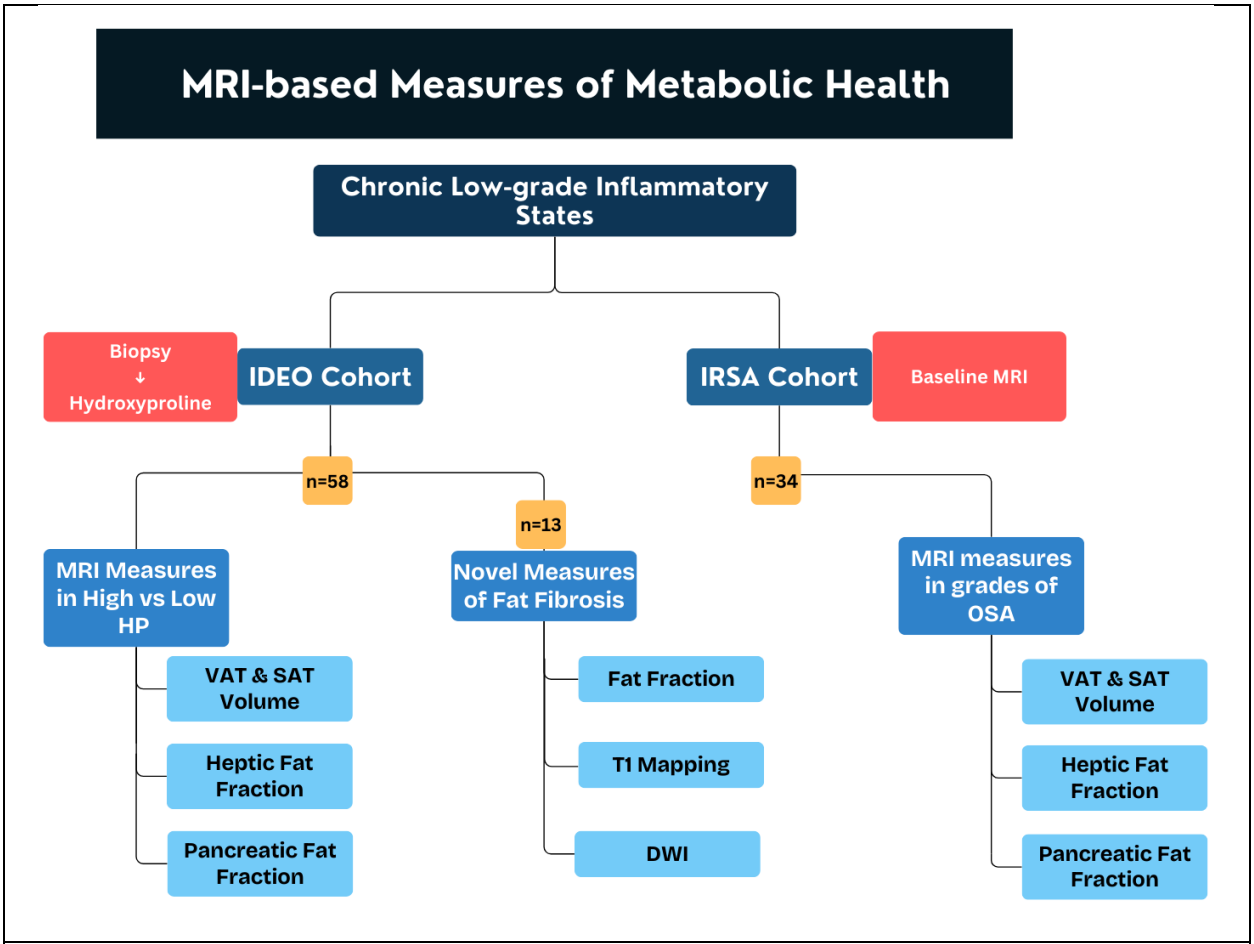

Fig. 3.1: Schematic diagram of the study design. Subjects are derived from two different cohorts and compared with the same MRI metrics against their respective independent variables. A subset of participants from the IDEO cohorts are analyzed with exploratory MRI techniques to test their ability to detect and quantify fibrosis.

3.2 – MRI Techniques

MRI scans of all the participants were done with a General Electrical (GE Healthcare, Chicago, IL, USA)) Signa Premier 3T scanner. Fat fraction imaging of the abdomen was done using the IDEAL-IQ method. The IDEAL method (iterative decomposition of fat and water with echo asymmetry and least square estimation) is a multi-echo proton density fat fraction measurement method. Automatic processing on the scanner outputs images for fat, water, in-phase, out-of-phase, R2* (= 1/T2*, where T2* is an MR relaxation time),

and a proton density fat fraction map (PDFF). The scan parameters used for fat fraction imaging are described below.

The IDEAL-IQ sequence was run with a 10 mm and 5 mm slice thickness. The 5 mm thick slices were used for manually segmenting the pancreas. The 3D 10mm sequence had a repetition time (TR) of 7.04 milliseconds with 6 echoes and a flip angle of 3 degrees. It had a field of view (FOV) of 50 cm, and a NEX of 0.75. It had 256 frequency encodes and 128 phase encoding steps, with the final image having an in-plane resolution of 1.95 x 1.95 mm. The 5 mm slices had similar parameters to the 10 mm slices, except with a TR of 7.10 milliseconds and a flip angle of 4 degrees.

The DWI that was done on fat had b-values of b=2000 and b=3000 s/mm^2. This was done on the fat frequency spectrum to measure the diffusion of fat. The TR, FOV, NEX, slice thickness, and slice gap were 1800 milliseconds, 50 cm, and 2 for each b-value, 8 mm, and 2 mm, respectively. The diffusion measurement was done on fat by shifting the center frequency by 440 Hz. The fat diffusion measurements were done in three directions.

The T1 mapping of the SAT was done in a single slice in the umbilical region and using a saturation recovery pulse sequence. This used a flip angle of 45 degrees with inversion times (TIs) of 198, 343, 488, 633, 1833, 3032, 4233 ms and one acquisition without an inversion time. The FOV and slice thickness were 50 cm and 10 mm, respectively. The intensity images were then processed into T1 maps during analysis.

CHAPTER 4 – OBSTRUCTIVE SLEEP APNEA COHORT:

4.1 – Cohort:

This study involved two cohorts. The first cohort was from the "Insulin Resistance and Sleep Apnea: The Role of Hypoxia" study (Krystal and Schwarz et al.). This study recruited participants with varying degrees of obstructive sleep apnea. Laboratory tests were performed to measure multiple metabolic health variables like insulin level, fasting blood glucose, lipid panel, liver function test, etc. Then, the participants underwent multiparametric MRI and whole-body DXA scans to get image-based measurements of fat content in the abdomen and visceral organs. Our study compared the MRI-derived liver fat fraction, liver fat content, pancreatic fat fraction, and SAT and VAT fat volume at a consistent intervertebral level with the apnea-hypopnea index (AHI). The AHI is a continuous score that categorizes the severity of obstructive sleep apnea. This helped us gain insight into the variability in fat deposition as a function of disease severity.

4.2 – Image Processing Pipeline:

To meet the objectives of the OSA cohort, the analysis had to be done on the fat fraction images. The fat and water images generated from the 10 mm IDEAL-IQ sequence were converted into fat fraction (FF) maps offline that were scaled by a factor of 10 to provide a higher dynamic range and to better visualize the structures. The pixel value from these scaled fat fraction maps would be in units of 0.1% and help better highlight subtle fat fraction changes. The regions of interest were segmented on the FF-10 images (scaled fat fraction images).

The liver segmentation was done using a pre-trained convolutional neural network (CNN) model.[19] The model used in-phase, out-of-phase, R2*, and FF-10 images to segment the liver semi-automatically (Figure 4.1). The initial slices and the end slices of the liver, and the last slice where the heart is visualized close to the liver, are prescribed to the CNN. This method provided consistency across cases without any observer bias that could happen with manual segmentation.

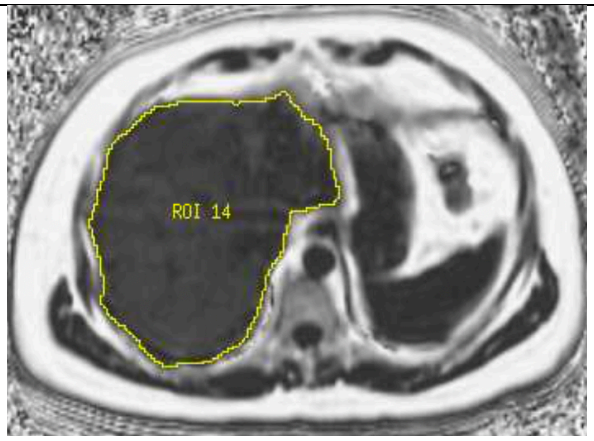

Fig. 4.1: CNN-based segmentation of the liver. The image shows the segmentation of the CNN overlaid on the Fat Fraction map. The model was able to successfully isolate the border of the liver without picking up other organs.

The SAT and the VAT segmentations were also done using a pre-trained CNN model (Figure 4.2), which used the same approach as the liver segmentation CNN. The pancreatic segmentation (Figure 4.3) was done manually on the 5 mm scaled fat fraction maps. This manual method is a process that has been tested previously for inter-user and intra-user validity.[20] Three sizes that had the best coverage of the pancreas were selected, and the center slice was selected to begin the segmentation. The region of interest (ROI) was drawn in a way that it was at least one voxel away from visceral fat in all three dimensions. The ROI drawn on the center slice was compared with the slices before and

after it. The ROI was edited to exclude fat in those slices. The smaller ROI, which does not cover fat in all three slices, is finally overlaid on the center slice, and the fat fraction is measured. This method ensured that the ROI measures just the fat fraction of the pancreatic parenchyma, and the measurement is not affected by visceral fat.

Fig. 4.2: CNN-based segmentation of the subcutaneous and visceral adipose tissue. The image shows the segmentation of the CNN as a binary image. The measurements on SAT and VAT were done after overlaying the mask on a fat fraction map.

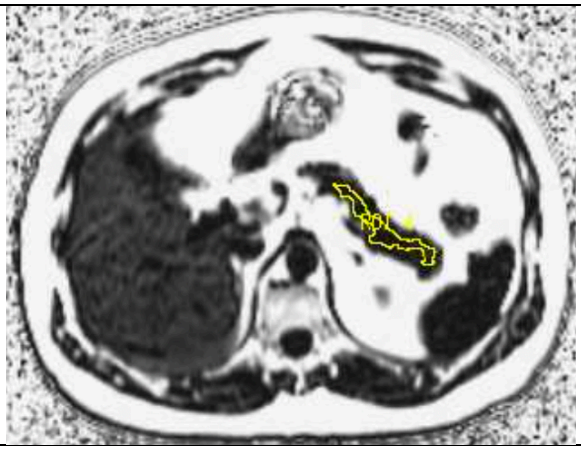

Fig. 4.3: Manual segmentation of the pancreas. The image shows the segmentation of the pancreas overlaid on a 5 mm fat fraction map. Care was taken by the operator to not include visceral fat in the segmentation.

4.3 – Analysis:

Statistical analysis was done on various measures derived from superimposing the segmentations from the liver, pancreas, subcutaneous adipose tissue, and visceral adipose tissue. The dependent and independent variables being compared are outlined in Table 4.1. A description of the variables used in a secondary analysis that aimed to validate the utility of the MRI metrics is given in Table 4.2.

Table 4.1: Variables analyzed in the Obstructive Sleep Apnea cohort

INDEPENDENT VARIABLES	DEPENDENT VARIABLES
• Apnea-Hypopnea Index (AHI) Score • AHI – Categories (Mild, Moderate and Severe) • Oxygen Desaturation Time (in minutes)	• Liver Fat Fraction (in %) • Liver Fat Content (FF x Volume) (in cc) • Pancreatic Fat Fraction (in %) • SAT Volume at L3-L4 Level (in cc) • VAT Volume at L3-L4 Level (in cc)

The independent variables primarily analyzed for the OSA cohort were measures of disease severity. The most commonly and widely used measure of OSA severity is the apnea-hypopnea index (AHI). This is the average number of apneas and hypopneas per hour of sleep in patients with OSA. The AHI values can be further used to bin patients into severity categories. OSA patients can be categorized into mild (AHI of 5 to less than 15 events per hour), moderate (AHI of 15 to less than 30 events per hour), and severe (AHI of greater than 30 per hour).[21] An apnea is a drop in nasal airflow of 90% or more lasting at least 10 seconds. A hypopnea is a drop in nasal pressure of at least 30% for at least 10 seconds with a drop in oxygen saturation of at least 4%. The analysis of the OSA cohort compared the MRI metrics against AHI as a continuous score (in units of events per hour)

and as categories of mild, moderate, and high. Additionally, another metric called the oxygen desaturation time was measured. This is the number of minutes the patient had an oxygen saturation of 88% or less. The MRI metrics that were compared as the dependent variables were the mean liver fat fraction (as a percentage), mean pancreatic fat fraction (as a percentage), SAT, and VAT volume at a consistent L3-L4 intervertebral level (in cc), and liver fat content (in cc). The liver fat content is a measure calculated as a product of the liver fat fraction and the segmented liver volume. This would give the fat content as a volume instead of a fraction.

Table 4.2: Variables used to validate MRI measures

INDEPENDENT VARIABLES	DEPENDENT VARIABLES
• Sex • BMI • HOMA-IR levels • HOMA-IR categories	• Liver Fat Fraction (in %) • Liver Fat Content (FF x Volume) (in cc) • Pancreatic Fat Fraction (in %) • SAT Volume at L3-L4 Level (in cc) • VAT Volume at L3-L4 Level (in cc)

As part of the secondary analysis, the same MRI metrics (liver fat fraction, liver fat content, pancreatic fat fraction, SAT, and VAT volume) were compared against standard clinical measures like sex and BMI. Furthermore, to verify if the chosen MRI metrics served as a good indicator of metabolic health, they were compared with a known clinical score of insulin resistance called the HOMA – IR (homeostatic model assessment for insulin resistance). This measure is a calculated value using the fasting insulin and glucose values measured as part of the metabolic panel that the OSA subjects underwent.

Using a linear regression method, the MRI metrics were compared with continuous variables like AHI score, oxygen desaturation time, BMI, and HOMA-IR levels. The correlation coefficient and the p-value were used to conclude whether each variable correlated with each MRI metric. The MRI metrics and each categorical independent variable underwent non-parametric comparisons for each pair using Wilcoxon's method. The p-value of the mean score difference of each metric between each pair of independent variables was calculated.

4.4 – Results:

4.4.1 – Cohort Demographics:

The obstructive sleep apnea cohort had an initial participant sample size of 34. The sample size of the analyzed group was 33. One participant was excluded because their lipid profile and liver enzyme results were deranged. Their liver fat fraction was also very high (41.05%), and further examination suggested a family history of liver disease. This caused a lot of confounding factors, which could affect the results, hence warranting the exclusion of this participant's data.

The sample size was 33, with 24 (72.7 %) males and 9 (27.3 %) females. The mean age of the participants was 49.3 years, with a maximum of 78 years and a minimum age of 28 years. The mean BMI was 32.08. Figure 4.4 shows the distribution of age, BMI, race, and ethnicity of the participants of the OSA cohort.

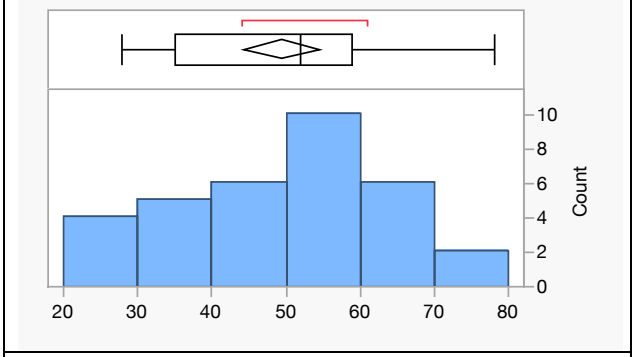

a. Distribution of Age

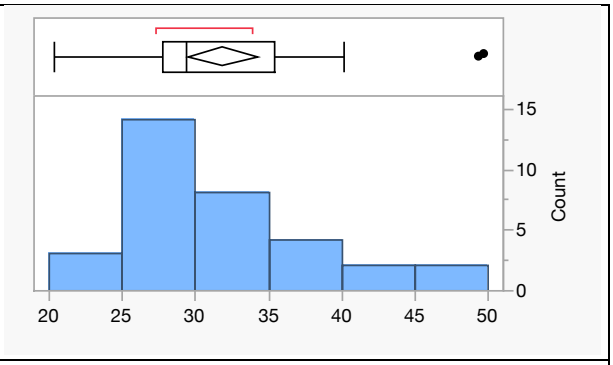

b. Distribution of BMI

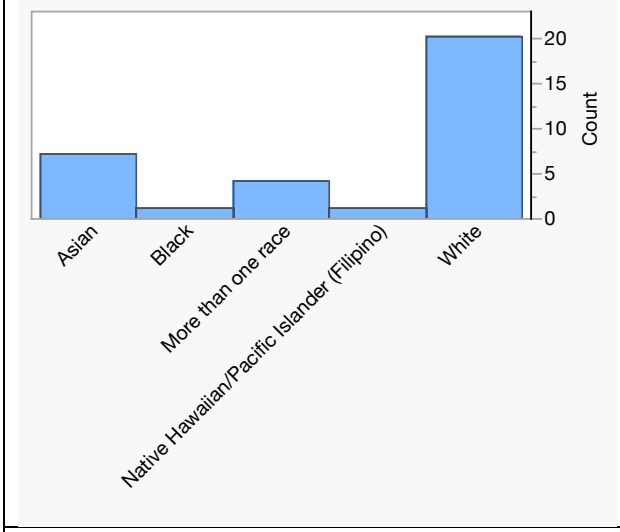

c. Distribution of Races

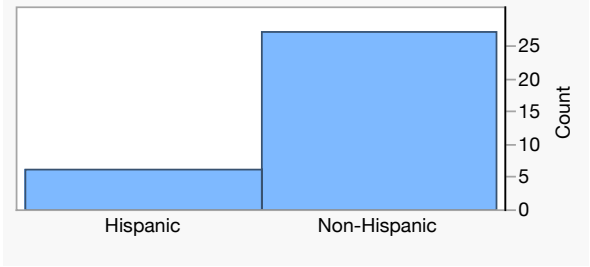

d. Distribution of Ethnicity

Fig. 4.4: Demographic data of the Obstructive Sleep Apnea Cohort

4.4.2 – Sleep Severity Metrics vs MRI measures:

The MRI metrics were initially compared against the AHI categories (mild, moderate, and severe). The liver fat fraction was significantly different between severe and moderate ($p=0.03$) and severe and mild ($p=0.01$) categories of participants. Liver fat content was significantly different between severe and moderate categories ($p=0.03$). Pancreatic fat, on the other hand, was significantly different between severe and mild categories ($p=0.02$). Overall, these measures of ectopic fat depositions in the liver and pancreas were consistently higher in the participant group with severe levels of OSA.

Interestingly, the SAT volume at L3-L4 intervertebral level was significantly different, only between mild and moderate categories (p=0.02). However, this was different, as participants with moderate OSA had lower SAT volume than those with mild OSA. The VAT volume at the L3-L4 level was similar between the different groups. The results of the one-way analysis between the significant variables discussed above are described as box plots in Figure 4.5.

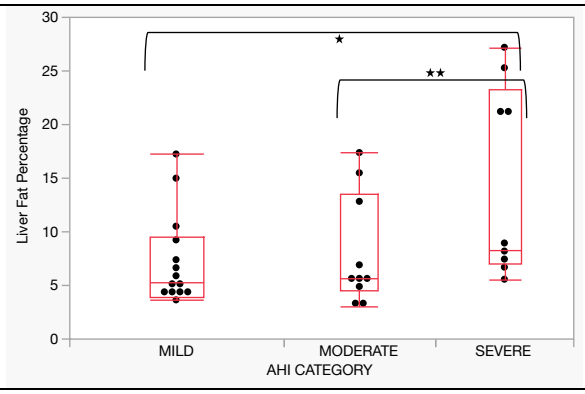

a. Liver Fat Fraction (in %) vs AHI Categories (*p=0.01, **p=0.03)

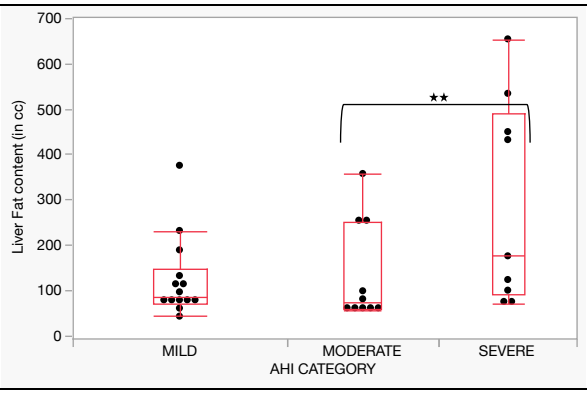

b. Liver Fat Content (in cc) vs AHI Categories (**p=0.03)

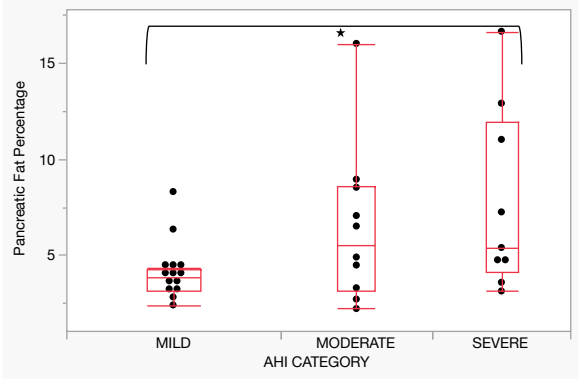

c. Pancreatic Fat Fraction (in %) vs AHI Categories (*p=0.02)

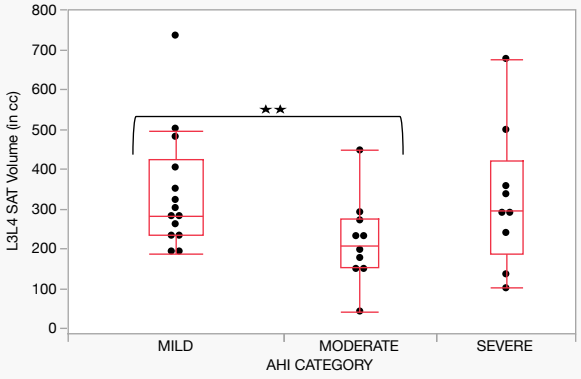

d. Subcutaneous Adipose Tissue Volume (in cc) vs AHI Categories (**p=0.02)

Fig. 4.5: Apnea-Hypopnea Index (AHI) Categories vs MRI Metrics in OSA

Similarly, the same metrics were compared against the AHI score as a continuous variable. The continuous AHI score was significantly positively correlated with liver fat fraction (p=0.01), liver fat content (p=0.005), and pancreatic fat fraction (p=0.003) (Figure 4.6). SAT and VAT volume at the L3-L4 level were not significantly correlated with the AHI score.

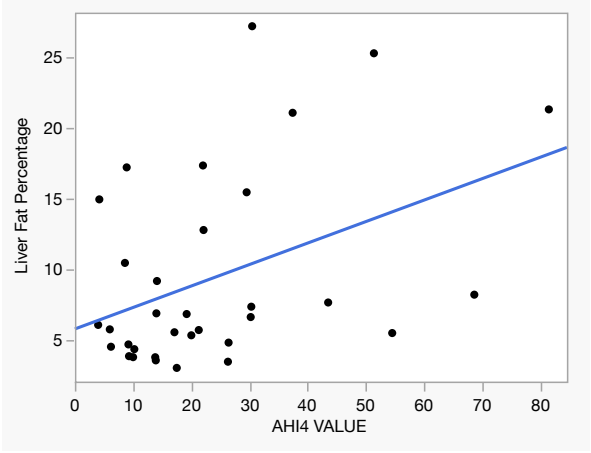

a. Liver Fat Fraction (in %) vs AHI Score (p=0.01)

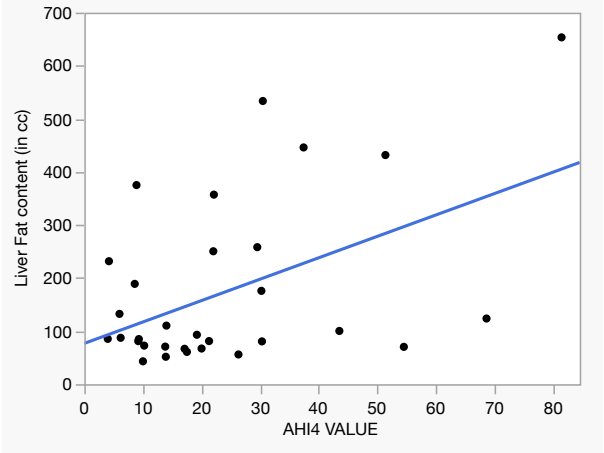

b. Liver Fat Content (in cc) vs AHI Score (p=0.005)

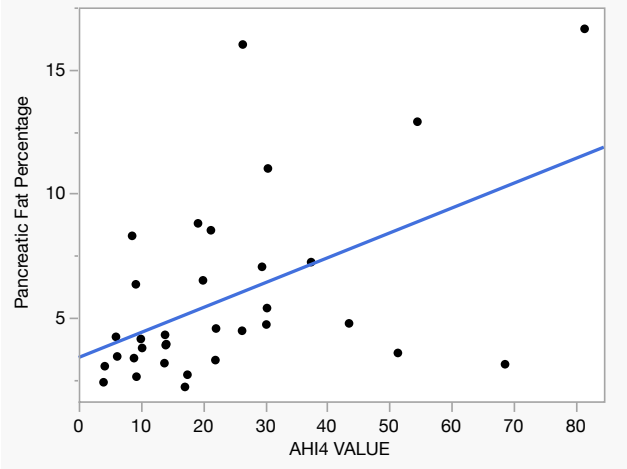

c. Pancreatic Fat Fraction (in %) vs AHI Score (p=0.003)

Fig. 4.6: Bivariate fit of AHI Score vs MRI Measures in OSA

Furthermore, when the metrics were compared against the oxygen desaturation time (in minutes), it was significantly correlated with liver fat fraction ($p=0.002$), liver fat content ($p<0.0001$), pancreatic fat fraction ($p=0.008$) and L3-L4 SAT volume ($p=0.02$). Time spent with less than 88% oxygen saturation was not significantly correlated with VAT volume. The correlation analysis between the oxygen desaturation times and the MRI measures is shown in Figure 4.7. One value of this metric was significantly higher than the others. When the analysis was rerun while excluding this value, the liver fat fraction and liver fat content were still significantly correlated while pancreatic fat fraction and SAT volume lost significance. On the other hand, VAT volume, which was not significant before, gained significance after the exclusion of this outlier.

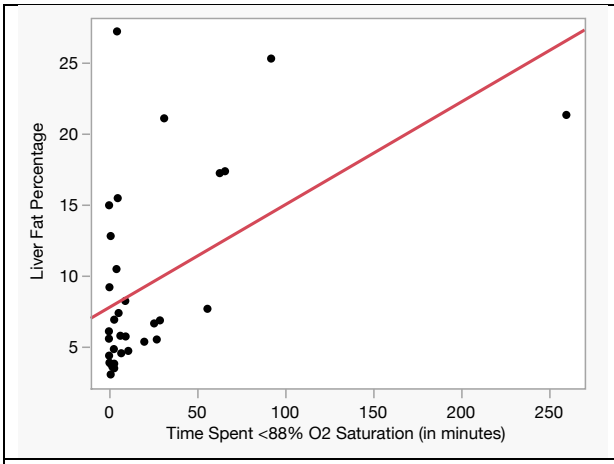

a. Liver Fat Fraction (in %) vs Oxygen Desaturation Time (p=0.002)

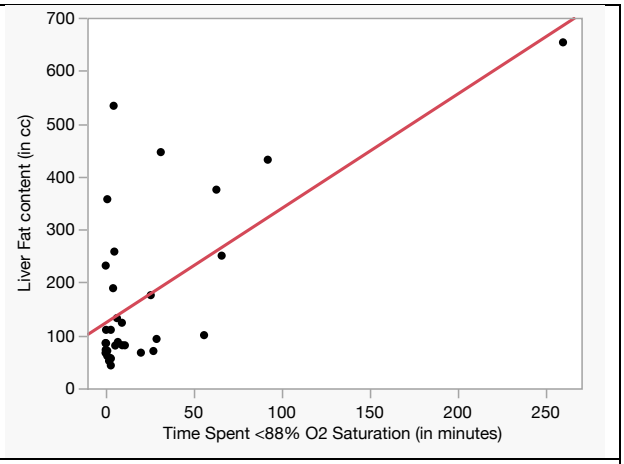

b. Liver Fat Content (in cc) vs Oxygen Desaturation Time (p<0.0001)

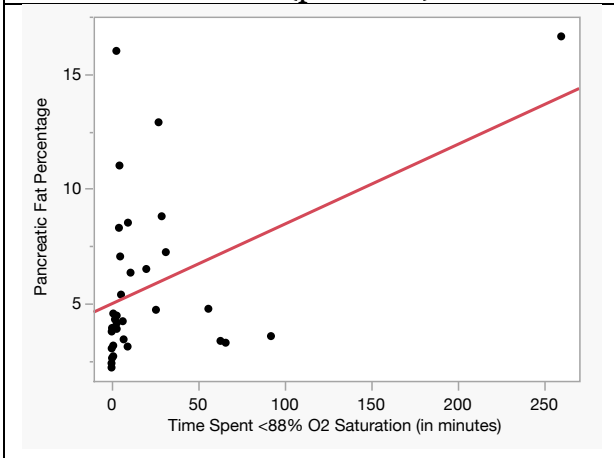

c. Pancreatic Fat Fraction (in %) vs Oxygen Desaturation Time (p=0.008)

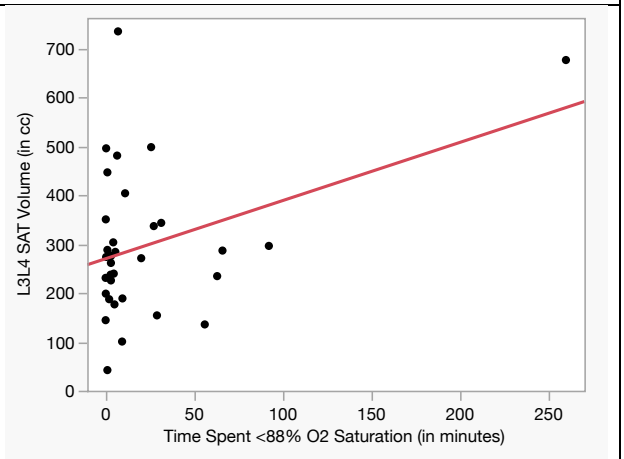

d. Subcutaneous Adipose Tissue Volume (in cc) vs Oxygen Desaturation Time (p=0.02)

Fig. 4.7: Oxygen Desaturation Time vs MRI Metrics in OSA

4.4.3 – MRI Measures Compared with Clinical Measures:

To verify the utility of the chosen MRI measures with clinical insulin resistance measures and whether other variables like sex and BMI confounded these measures, further analysis was done between MRI measures and other independent variables. The same MRI metrics were compared with BMI, sex, HOMA-IR levels, and HOMA-IR categories. HOMA-IR was categorized into high and low based on whether they are greater than or

equal to a chosen cut-off value. Multiple studies have varying suggestions for which value to use as a cut-off. Based on the scope of our study, we chose 2.2 as the cut-off value.[22] Analysis showed that in the OSA cohort, among the five metrics, only VAT volume at the L3-L4 level was significantly different between women and men. Men had significantly higher volumes of fat in Visceral adipose tissue than women (p=0.04). Other metrics were not affected by sex. BMI was significantly correlated with liver fat content (p=0.03), SAT volume (p<0.0001), and VAT volume (p=0.001). Liver fat fraction and pancreatic fat fraction were not significantly correlated to BMI. When compared to the HOMA-IR levels as a continuous variable, the liver fat fraction (p=0.01), liver fat content (p=0.01), SAT volume (p=0.008), and VAT volume (p=0.01) were positively correlated with it. Furthermore, the liver fat fraction (p=0.01), liver fat content (p=0.007), SAT volume (p=0.007), and VAT volume (p=0.02) were significantly higher in participants with HOMA-IR levels greater than 2.2.

Based on the linear fitting models of liver fat content to BMI, the liver fat content values were adjusted to account for BMI. This adjusted liver fat content was compared again with the AHI values. The adjusted liver fat content was still positively correlated with the AHI score (p=0.005) as a continuous variable.

4.5 – Discussion:

In the OSA cohort, the participants with higher AHI scores had significantly higher levels of liver fat fraction, liver fat content, and pancreatic fat fraction. These measures of ectopic fat deposition correlated with AHI as a continuous variable and significantly differed between different AHI categories. Of note, participants with severe OSA always had higher measures of ectopic fat. Visceral and subcutaneous adipose tissue volumes at

the L3-L4 vertebral level were not significantly different. Compared with clinical measures, VAT volume was significantly higher in males compared to females.

Furthermore, liver fat content and VAT volume were significantly correlated with BMI values. The positive correlation was still significant when liver fat was adjusted for BMI and then compared to AHI scores. Liver fat fraction, liver fat content, pancreatic fat fraction, and VAT volume were significantly correlated with HOMA-IR categories.

Ectopic fat deposition in the liver and the development of non-alcoholic fatty liver disease in association with OSA have been well documented.[23] While significant literature is available regarding ectopic depositions of fat in OSA, [24] its role in the development of fatty pancreas is an area of active research.[25] The results from this study corroborate literature that highlights the sensitivity of MRI-PDFF in measuring and quantifying fat depositions in the liver.[26] Additionally, the liver fat content as a metric is useful in quantifying fat in the liver in the context of its volume. The results of this study with respect to pancreatic fat highlight the utility of PDFF in measuring pancreatic fat and demonstrate this additional metric of poor metabolic health associated with OSA and OSA severity.

CHAPTER 5 – IDEO COHORT:

5.1 – Cohort:

The second cohort was derived from the "Inflammation, Diabetes, Ethnicity and Obesity (IDEO) Cohort" study (Koliwad et al.). This study involved the development of a multiethnic cohort with obesity and inflammation. The cohort contained participants with and without HIV infection. The participants underwent abdominal fat biopsy as part of the multi-panel metabolic assessment. This sample was then tested for hydroxyproline. This amino acid is an essential building block of collagen and can serve as a biomarker for fibrosis.[27] These participants also underwent multiparametric MRI scans of the abdomen. The same MRI metrics analyzed for the first cohort were compared against the IDEO cohort's hydroxyproline levels. MRI metrics were also compared against other clinical measures like sex, BMI, lipid profile, etc.

5.2 – Image Processing Pipeline and Analysis:

The image processing pipeline used to analyze the IDEO cohort was similar to what was done for the OSA cohort (described in Section 4.2). However, the key changes in the analysis were based on the independent variables used to compare the MRI metrics. While the OSA cohort was compared with the AHI score as a severity measure, the hydroxyproline value derived from the abdominal fat biopsy was the variable of interest in the IDEO cohort. The independent and dependent variables that were compared in the IDEO cohort are described in Table 5.1.

Table 5.1: Variables analyzed in the Inflammation Diabetes Ethnicity and Obesity cohort	
INDEPENDENT VARIABLES	**DEPENDENT VARIABLES**
• Hydroxyproline Levels (in ng/mg) • Hydroxyproline levels as categories (High vs Low)	• Liver Fat Fraction (in %) • Liver Fat Content (FF x Volume) (in cc) • Pancreatic Fat Fraction (in %) • SAT Volume at L3-L4 Level (in cc) • VAT Volume at L3-L4 Level (in cc)

Hydroxyproline levels were plotted against the MRI measures as a continuous variable in units of ng/mg and as categorical groups of low and high hydroxyproline. Limited work exists for which value to choose as a cut-off for high hydroxyproline and its association with insulin resistance.[28] A 350 ng/mg cut-off was used to define high and low hydroxyproline in the cohort. On preliminary analysis of hydroxyproline levels with metabolic measures such as lipid profile, insulin, and HbA1c, these measures were higher in Hydroxyproline values in the 300 to 400 ng/mg range. Hence, 350 ng/mg was chosen as the arbitrary cut-off to compare with MRI measures. The secondary analysis of the measures with the clinical variables like sex, age, and HOMA-IR was also done on this cohort, similar to what is described in Table 4.2. The continuous variables were compared using linear regression, and the categories of hydroxyproline levels were compared non-parametrically using the Wilcoxon method.

5.3 – Results:

5.3.1 – Cohort Demographics:

The sample size of the participants who were analyzed from the IDEO cohort was 58. This sample was split into 42 males (72.4%) and 16 females (27.6%). The mean age of the sample was 50.5 years, with a maximum age of 71 years and a minimum age of 23 years. The mean BMI was 27.9, with an outlier of 64.6. Among the participants of this cohort, 67.24 % of them had a HIV-positive status. Figure 5.1 depicts the demographic data of the IDEO cohort.

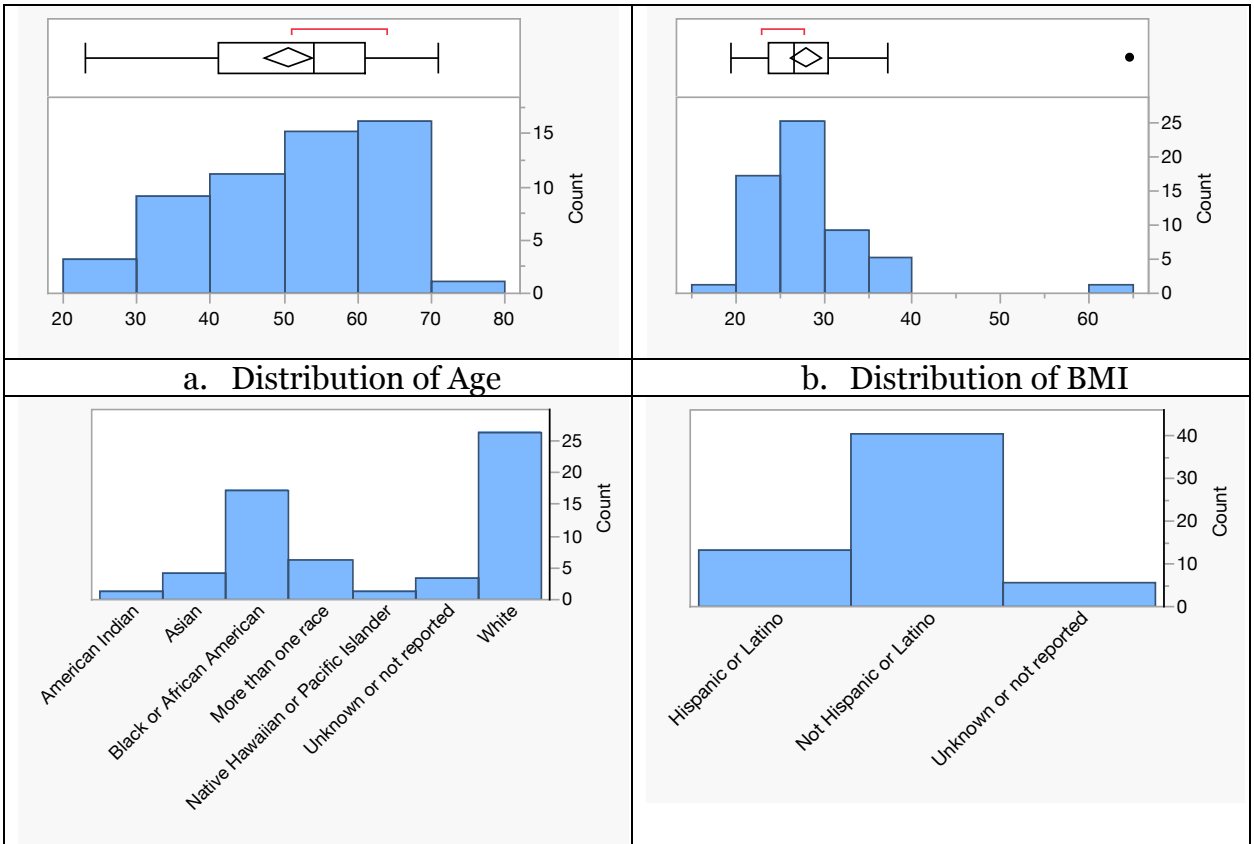

a. Distribution of Age

b. Distribution of BMI

c. Distribution of Races

d. Distribution of Ethnicity

Fig. 5.1: Demographic data of the IDEO Cohort

5.3.2 – Hydroxyproline Levels vs MRI Metrics:

As mentioned in the previous section, liver fat fraction, liver fat content, pancreatic fat fraction, SAT volumes, and VAT volumes at the L3-L4 level were compared with hydroxyproline groups and values. When compared with the Hydroxyproline categories, the liver fat fraction ($p=0.03$), pancreatic fat fraction ($p=0.03$), SAT volume ($p=0.01$), and VAT volume ($p=0.002$) were higher in the high hydroxyproline groups. Liver fat content was not significantly different between both groups. Compared with the Hydroxyproline level as a continuous variable and analyzed using linear regression, SAT volume ($p=0.003$) and VAT volume ($p=0.007$) were significantly positively correlated. The other metrics, such as liver fat fraction, liver fat content, and pancreatic fat fraction, were not correlated with continuous hydroxyproline levels. These results are described using box plots and linear graphs in Figure 5.2.

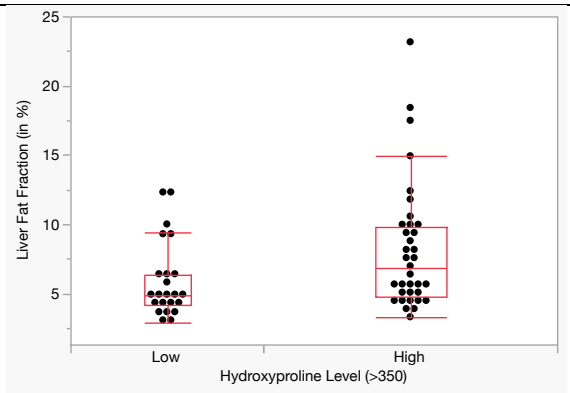

a. Liver Fat Fraction (in %) vs Hydroxyproline Categories (p=0.03)

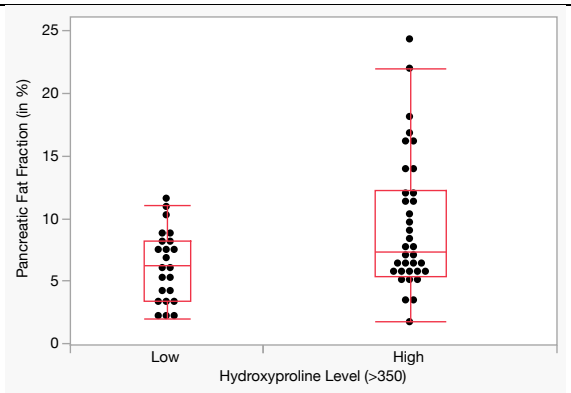

b. Pancreatic Fat Fraction (in %) vs Hydroxyproline Categories (p=0.03)

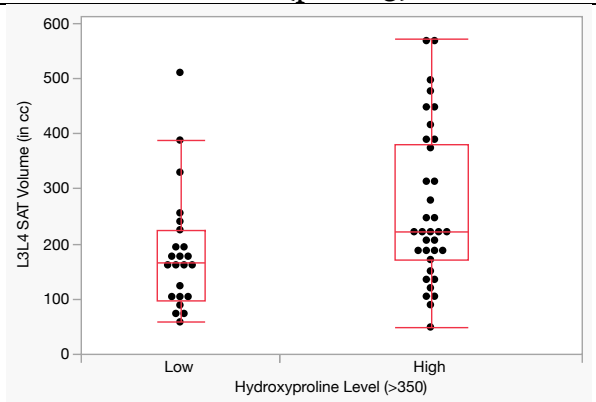

c. Subcutaneous Adipose Tissue Volume (in cc) vs Hydroxyproline Categories (p=0.01)

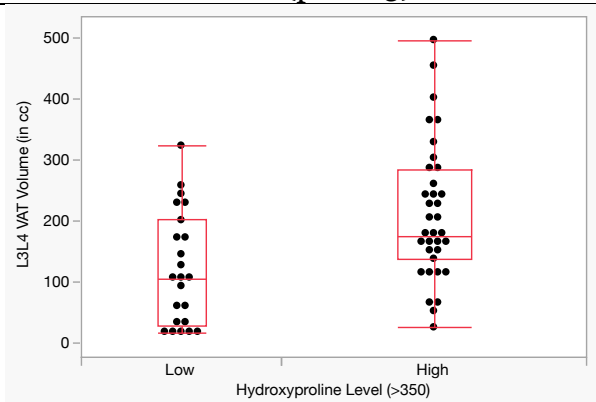

d. Visceral Adipose Tissue Volume (in cc) vs Hydroxyproline Categories (p=0.002)

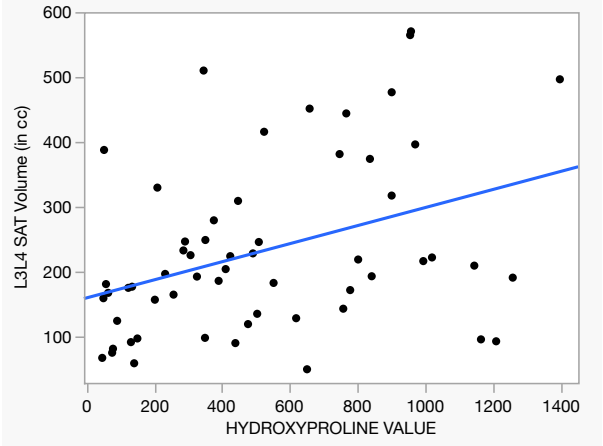

e. Subcutaneous Adipose Tissue Volume (in cc) vs Hydroxyproline levels (in ng/mg) (p=0.003)

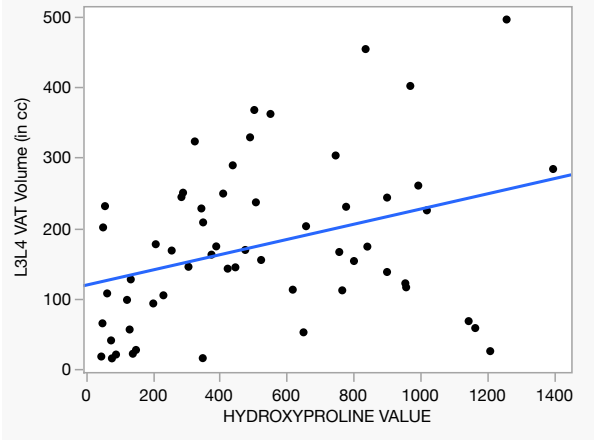

f. Visceral Adipose Tissue Volume (in cc) vs Hydroxyproline levels (in ng/mg) (p=0.007)

Fig. 5.2: Hydroxyproline vs MRI metrics in IDEO Cohort

5.3.3 – MRI Measures Compared with Clinical Measures:

As described in section 4.4.3, the MRI metrics were also compared with clinical metrics in the IDEO cohort. The liver fat fraction, liver fat content, pancreatic fat fractions, and adipose tissue volumes were compared against sex, BMI, HOMA-IR categories, and HOMA-IR levels. In the IDEO cohort, there were no significant sex differences in liver fat fraction, liver fat content, pancreatic fat fraction, VAT, and SAT volumes. Analysis with the BMI values showed that SAT volume ($p<0.0001$) and VAT volume ($p<0.0001$) were significantly and positively correlated. Liver fat fraction ($p<0.0001$), liver fat content ($p<0.0001$), pancreatic fat fraction ($p=0.02$), SAT volume ($p=0.03$), and VAT volume ($p<0.0001$) were significantly higher in participants with higher HOMA-IR level (>2.2). All these metrics were also positively correlated with HOMA-IR as a continuous measure with p-values of 0.001, 0.002, 0.01, 0.007, and <0.0001, respectively.

To adjust for the variability in MRI metrics due to BMI, the cohort was divided into two categories of high and low BMI values (using a cut-off value of 25). Analysis was performed on the two groups separately for correlation between MRI metrics and hydroxyproline values. The differences in metrics were not significant in the high BMI category. However, in the low BMI category, the VAT volume ($p=0.02$), liver fat fraction ($p=0.03$), and liver fat content ($p=0.02$) were all significantly higher in the high hydroxyproline group.

5.4 – Discussion:

In the IDEO cohort, liver fat fraction, pancreatic fat fraction, and VAT volume significantly differed between participants with high and low hydroxyproline levels on their abdominal fat biopsy. These ectopic fat measures were significantly higher in participants with higher hydroxyproline levels. SAT and VAT volumes were also significantly correlated with hydroxyproline levels as a continuous variable. The sex differences in VAT in the OSA cohort were not seen in the IDEO cohort. VAT volume was correlated with BMI, while liver fat fraction, liver fat content, and VAT volume were significantly correlated with HOMA-IR categories. When the cohort was divided into groups with high BMI and low BMI, it was seen that VAT volume was not correlated with hydroxyproline level in the high BMI group. However, in the low BMI group, the liver fat fraction, liver fat content, and VAT volume were significantly higher in participants with high hydroxyproline levels.

Literature suggests that fat fibrosis is associated with poor metabolic health and the deposition of fat in the liver.[29][30] There are no studies that correlate fat fibrosis and fatty pancreas. The results from this study emphasize the point of ectopic fat measures being higher in people with higher fat fibrosis. Studies suggest that fibrosis alters the extracellular matrix of the subcutaneous adipose tissue. This would mean that it would also impair its function. It is reasonable to conclude that fat storage in these cases of fibrosis is higher in the visceral compartment. This theory is consolidated by the results from this study that VAT volume is higher in people with fibrosis. Additionally, the grouping of participants based on BMI and analysis shows that this effect is more significant in leaner people.

CHAPTER – 6: NOVEL MEASURES OF FAT FIBROSIS DETECTION:

6.1: Cohort:

The cohort selection for running the exploratory analysis of fat fibrosis using Diffusion-weighted imaging and T1 mapping was different from the other analyses. Even though the subjects for this analysis were selected from the IDEO cohort, T1 maps with the same protocol and DWI with high b-values on fat (b=2000 and b=3000 s/mm^2) were not present in all these subjects. Hence, a sample size of n=16 was chosen to analyze DWI. For the T1 mapping, data from 13 participants was analyzed. Fat fraction maps were available for a wider sample of participants. FF median and FF mode of the SAT at L3-L4 level were analyzed for 58 participants. All these metrics were compared with the hydroxyproline levels and categories.

6.2 Image Processing Pipeline:

ADC maps for both b=2000 s/mm^2 and b=3000 s/mm^2 were generated. These maps were calculated using the intensities of diffusion images of b=2000 s/mm^2 and b=0, and b=3000 s/mm^2 and b=0. Diffusion images for each b-value were taken in three different directions. The maps were computed as the geometric mean of the ADC values in all these directions. Figure 6.1 shows an example of the b=3000 s/mm^2 ADC maps.

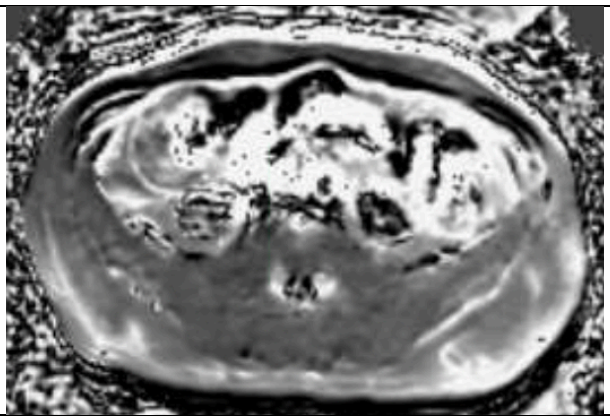

Fig. 6.1: ADC map generated from Diffusion-Weighted Imaging of fat with b=3000 s/mm²

The T1 maps were generated from the intensity images from the saturation-recovery T1 mapping protocol. Each image from the T1 mapping protocol has nine volumes, with each volume corresponding to a different inversion time. A linear fitting method was developed to calculate the T1 value of each pixel from the slice. The linear fitting was done using the intensity values of the corresponding pixel from the nine volumes with different inversion times. A MATLAB (MATLAB, Version R2023A, Natick, MA, USA) code was developed to calculate the T1 map using this method. An image of the T1 map generated from this method is shown in Figure 6.2. Fat fraction maps of the SAT were generated the same way as those mentioned in the processing pipeline for the previous analysis. SAT was segmented using the same CNN discussed previously. However, to avoid edge artifacts and noise in the peripheral regions of the SAT, a morphological erosion was done to the CNN-generated SAT segments, such that only a small segment from the deep SAT, which is devoid of any artifact or noise effect, is selected for analysis of ADC and T1 values. Figure 6.3 shows an eroded ROI that segments a region from the deep SAT. The median FF value of the SAT was analyzed to avoid the same problem of the region of interest (ROI) picking up unwanted edge artifacts. The mean is altered by these edge pixels, but

the median is a more robust measure less affected by outliers. Hence, the median fat fraction from the SAT was analyzed.

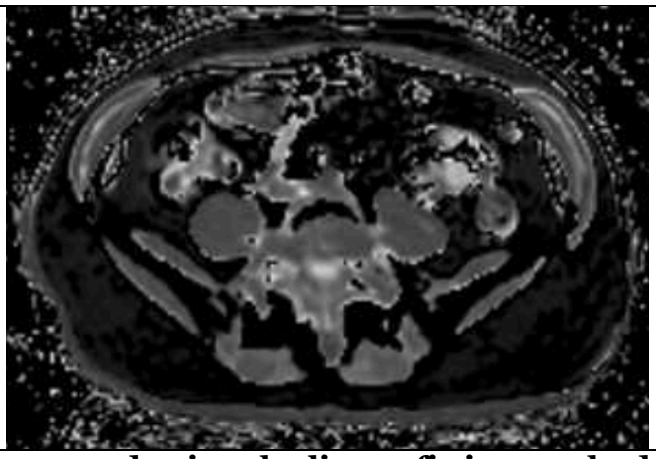

Fig 6.2: T1 map computed using the linear fitting method

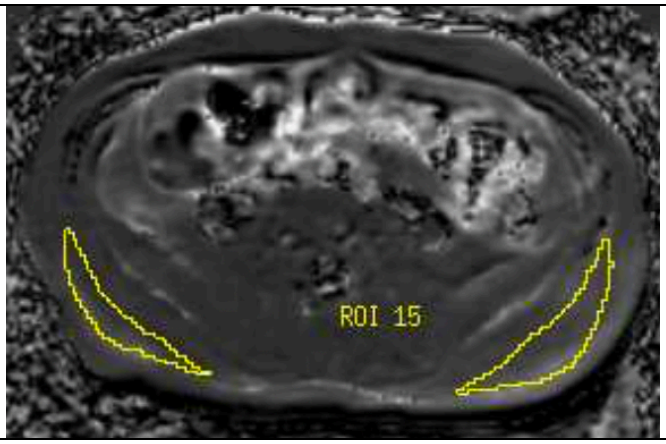

Fig 6.3: ADC map with the eroded SAT segmentation overlaid

6.3 – Analysis:

The analysis for this exploratory section of the study was done on three sets of variables compared against the Hydroxyproline levels as continuous and categorical variables. Table 6.1 outlines the independent and dependent variables used for this analysis. The dependent variables that were used were ADC values (both with b=2000 and b=3000

s/mm²) (n=16), the median T1 values (n=13) from the eroded SAT segments, and the median fat fraction of the SAT (n=58). The continuous independent variables are analyzed using linear regression. The categorical variables are analyzed using the non-comparison of each pair using the Wilcoxon method.

Table 6.1: Variables compared for exploratory analysis to detect fibrosis

INDEPENDENT VARIABLES	DEPENDENT VARIABLES

• Hydroxyproline Levels (in ng/ml)
• Hydroxyproline levels as categories (High vs Low)
	• ADC Values on SAT (in $\times 10^{-6}$ mm²/s)
	  • ADC2000
	  • ADC3000
	• Median T1 values on SAT (in msec)
	• Median Fat Fraction of SAT (in %)

6.4 – Results:

The non-parametric comparison of the high and low hydroxyproline categories showed no statistically significant difference between groups in ADC-2000 and ADC-3000 values. However, a decreasing trend in both ADCs could be seen between low and high groups. When the ADC values were analyzed against hydroxyproline levels as a continuous variable, the ADC-3000 values were significantly negatively correlated (p=0.04). The ADC-2000 values also decreased with increasing values of hydroxyproline, but this did not reach levels of statistical significance (p=0.16). Some of these findings from the ADC analysis are depicted in Fig. 6.4.

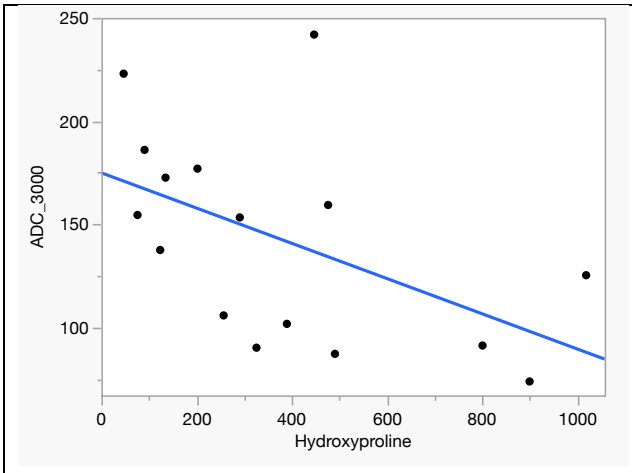

a. Mean ADC-3000 of Subcutaneous fat vs Hydroxyproline levels (p=0.04)

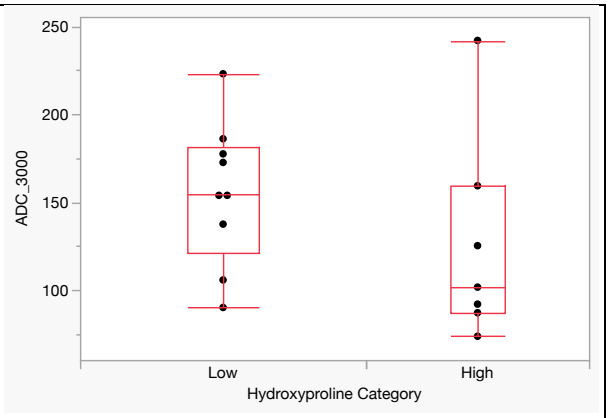

b. Mean ADC-3000 ($\times 10^{-6}$ mm^2/s) of Subcutaneous fat vs Hydroxyproline categories (p=0.16)

Fig. 6.4: Analysis of ADC-3000 against Hydroxyproline Values

Analysis of the Median T1 values against the Hydroxyproline levels showed no significant difference. An overall decreasing trend of the median T1 values with increasing Hydroxyproline was seen; however, it was not statistically significant (p=0.6). Similarly, the median fat fraction of the SAT was neither significantly different with different categories of hydroxyproline nor significantly correlated with hydroxyproline values as a continuous variable.

There were 13 cases with values for all three parameters (ADC3000, median T1, and median FF of SAT). A preliminary stepwise nominal regression modeling was done to show promising results in identifying participants with high hydroxyproline levels. The stepwise modeling was done using JMP Statistical Discovery software (JMP Pro, Version 18, SAS Institute Inc., Cary, NC, USA). The stopping parameter for the model was a p-value threshold. The p-value to enter was 0.25, and the p-value to leave was set at 0.2.

The whole model had a p-value of 0.01. The ADC 3000 and median T1 measures were selected, with the ADC3000 having the greatest effect in improving the model's performance. The Receiver-Operating Curve (ROC) was plotted (Figure 6.5), showing the model's capability to identify cases with high hydroxyproline. The area under the curve (AUC) was 0.928.

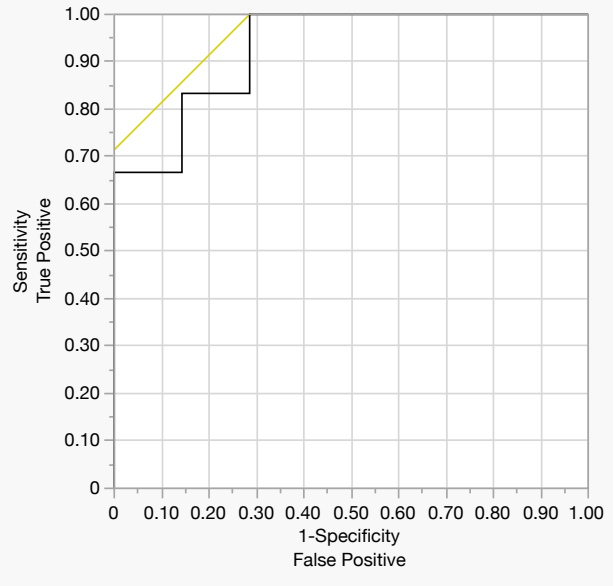

Fig. 6.5: Receiver-Operating Curve (ROC) of model using ADC3000 and T1 values of SAT to identify high hydroxyproline levels (>350 ng/mg)

6.5 – Discussion:

The preliminary analysis of the novel measures, such as the ADC measurement of SAT and T1 values using T1 mapping of SAT and SAT fat fraction, was promising. The most significant was the positive correlation between ADC-3000 values and hydroxyproline levels as a continuous variable. ADC-2000 did show a decreasing trend with higher hydroxyproline, but this did not reach levels of statistical significance. The median T1 values of the SAT did show a decrease between high and low hydroxyproline levels, but they were not significant. The fat fraction values were similarly not significant. Combining

these three variables into a model to predict high hydroxyproline in SAT showed encouraging results, with a significant p-value and an AUC-ROC of 0.93. Limited sample size would be the biggest limitation in this part of the study. While the trends seem in line with what was expected from the literature, their not reaching levels of significance could be because of the limited sample size being analyzed. The promise of these measures in detecting fibrosis suggests that they could benefit from further analysis of more participants with uniform scanning protocols.

CHAPTER – 7: CONCLUSION:

7.1 – Implications:

The comparison of the chosen MRI metrics against standard measures of insulin resistance and poor metabolic health, like HOMA-IR[31], showed that they are useful in getting valuable quantitative data on deranged metabolism. They were significantly associated across both cohorts. Liver fat measures (fat fraction and fat content) and pancreatic fat fraction were consistently higher in groups with poor metabolic outcomes (defined by high AHI values in OSA and high hydroxyproline levels in IDEO). One interesting observation in the IDEO cohort was the higher levels of visceral fat volume in participants with high levels of hydroxyproline on SAT. One possible explanation could be that impaired fat storage in the SAT contributes to its deposition in the visceral adipose tissue and other organs like the liver and pancreas. At the same time, when the subjects were grouped based on high and low BMI, the fat-depositing effect of SAT fibrosis was more significant in low BMI participants. This seems to imply that SAT fibrosis in someone already obese does not worsen their visceral adiposity, but fibrosis in a lean person has poorer metabolic outcomes.

The ADC measurements with a b-value of 3000 s/mm^2 had the best utility in measuring fat movement and hence had the best results in measuring restricted fat diffusion due to fibrosis. The diffusion of fat with high gradients is restricted by fibrosis - potentially because the size of the largest possible fat droplets may be limited when fibrosis is present. The T1 values were not significant but showed a decreasing trend. There is potential for this to be explored further with a larger sample size. The combined model in identifying

fibrosis was promising in its performance and has the potential to be improved with a larger sample size.

7.2 – Strengths and Limitations of the Study:

The semi-automated nature of segmenting the liver, SAT, and VAT had the benefit of nullifying operator bias during segmentation. Proton density fat fraction, the primary imaging modality used, had the advantage of being a quantitative and objective measure of fat content in the tissue. One limitation of the study is that the reference standards we used may have errors. AHI measures were determined from a single night's sleep study and may differ from a typical night for the subject, affecting our comparisons to the AHI data. For instance, one of the data points in the analysis between MR metrics and oxygen desaturation time (below 88%) was significantly higher than the others. While there is a possibility that it indeed was a true reading, it is not implausible that the pulse oximeter sensor just fell off the patient's finger while asleep. Hence, factors like this have the potential to alter our results. Additionally, the hydroxyproline measures were taken from an anterior biopsy, while our novel measures in the subcutaneous fat were generally from the deep subcutaneous fat in the posterior region. It is possible fibrosis is not uniform throughout the fat, impacting our comparisons to the hydroxyproline levels. The most significant limitation of the study is the need for a large sample size with uniform measurements for ADC and T1 measurements. While they showed promise, they were limited by the small sample size being analyzed. Furthermore, T1 measures are estimated using a linear estimation method without taking into account offset to the data and with an assumption of monoexponential relaxation, which may not reflect the actual behavior.

While this method is valuable in detecting trends with respect to hydroxyproline levels, a more advanced fitting method may detect more subtle differences.

7.3: Conclusion:

It can be concluded that subjects with worse grades of obstructive sleep apnea had worse measures of metabolic health compared to those with milder forms. Subjects with fibrosis in subcutaneous adipose tissue had higher measures of ectopic fat. Measures correlated with BMI were significantly associated with fibrosis of SAT in low BMI patients but not in high BMI patients. This suggests that SAT fibrosis in lean subjects is a risk factor for worse metabolic health. The promising pilot results of fat ADC with high b-values and T1 values using T1 mapping suggest these may be able to noninvasively detect fibrosis in subcutaneous fat once evaluated with larger study populations.

REFERENCES:

[1] World Health Organization: WHO. Noncommunicable diseases. Published September 16, 2023. https://www.who.int/en/news-room/fact-sheets/detail/noncommunicable-diseases

[2] Eckel RH. The Metabolic Syndrome. In: Loscalzo J, Fauci A, Kasper D, Hauser S, Longo D, Jameson J. eds. *Harrison's Principles of Internal Medicine, 21e*. McGraw-Hill Education; 2022. Accessed August 22, 2024. https://accessmedicine.mhmedical.com/content.aspx?bookid=3095&sectionid=265446328

[3] Tylutka A, Morawin B, Walas Ł, Michałek M, Gwara A, Zembron-Lacny A. Assessment of metabolic syndrome predictors in relation to inflammation and visceral fat tissue in older adults. *Scientific Reports*. 2023;13(1). doi:10.1038/s41598-022-27269-6

[4] Cen M, Song L, Fu X, Gao X, Zuo Q, Wu J. Associations between metabolic syndrome and anxiety, and the mediating role of inflammation: Findings from the UK Biobank. *Brain Behavior and Immunity*. 2024;116:1-9. doi:10.1016/j.bbi.2023.11.019

[5] de Araujo Dantas AB, Gonçalves FM, Martins AA, et al. Worldwide prevalence and associated risk factors of obstructive sleep apnea: a meta-analysis and meta-regression. *Sleep Breath*. 2023;27(6):2083-2109. doi:10.1007/s11325-023-02810-7

[6] Ryan S. Adipose tissue inflammation by intermittent hypoxia: mechanistic link between obstructive sleep apnoea and metabolic dysfunction. *J Physiol*. 2017;595(8):2423-2430. doi:10.1113/JP273312

[7] Safrin S, Grunfeld C. Fat distribution and metabolic changes in patients with HIV infection. *AIDS*. 1999;13(18):2493-2505. doi:10.1097/00002030-199912240-00002

[8] DeBari MK, Abbott RD. Adipose Tissue Fibrosis: Mechanisms, Models, and Importance. *Int J Mol Sci*. 2020;21(17):6030. Published 2020 Aug 21. doi:10.3390/ijms21176030

[9] Ibrahim MM. Subcutaneous and visceral adipose tissue: structural and functional differences. *Obes Rev*. 2010;11(1):11-18. doi:10.1111/j.1467-789X.2009.00623.x

[10] Zarghamravanbakhsh P, Frenkel M, Poretsky L. Metabolic causes and consequences of nonalcoholic fatty liver disease (NAFLD) [published correction appears in Metabol Open. 2023 Jan 21;17:100231. doi: 10.1016/j.metop.2023.100231]. *Metabol Open*. 2021;12:100149. Published 2021 Nov 16. doi:10.1016/j.metop.2021.100149

[11] Filippatos TD, Alexakis K, Mavrikaki V, Mikhailidis DP. Nonalcoholic Fatty Pancreas Disease: Role in Metabolic Syndrome, "Prediabetes," Diabetes and Atherosclerosis. *Dig Dis Sci*. 2022;67(1):26-41. doi:10.1007/s10620-021-06824-7

[12] Rinella ME, Lazarus JV, Ratziu V, et al. A multisociety Delphi consensus statement on new fatty liver disease nomenclature. *Hepatology*. 2023;78(6):1966-1986. doi:10.1097/HEP.0000000000000520

[13] Dixon WT. Simple proton spectroscopic imaging. *Radiology*. 1984;153(1):189-194. doi:10.1148/radiology.153.1.6089263

[14] Bray TJ, Chouhan MD, Punwani S, Bainbridge A, Hall-Craggs MA. Fat fraction mapping using magnetic resonance imaging: insight into pathophysiology. *Br J Radiol*. 2018;91(1089):20170344. doi:10.1259/bjr.20170344

[15] Reeder SB, Hu HH, Sirlin CB. Proton density fat-fraction: a standardized MR-based biomarker of tissue fat concentration. *J Magn Reson Imaging*. 2012;36(5):1011-1014. doi:10.1002/jmri.23741

[16] Noworolski SM, Lam MM, Merriman RB, Ferrell L, Qayyum A. Liver steatosis: concordance of MR imaging and MR spectroscopic data with histologic grade. *Radiology*. 2012;264(1):88-96. doi:10.1148/radiol.12110673

[17] Fukui H, Hori M, Fukuda Y, et al. Evaluation of fatty pancreas by proton density fat fraction using 3-T magnetic resonance imaging and its association with pancreatic cancer. *European Journal of Radiology*. 2019;118:25-31. doi:10.1016/j.ejrad.2019.06.024

[18] Franz D, Weidlich D, Freitag F, et al. Association of proton density fat fraction in adipose tissue with imaging-based and anthropometric obesity markers in adults. *Int J Obes (Lond)*. 2018;42(2):175-182. doi:10.1038/ijo.2017.194

[19] Gibbons M, Diaz EC, Koliwad S, et al. Combining convolutional neural networks, multiparametric MRI, and error detection to improve automated liver segmentation. *Proceedings on CD-ROM - International Society for Magnetic Resonance in Medicine Scientific Meeting and Exhibition/Proceedings of the International Society for Magnetic Resonance in Medicine, Scientific Meeting and Exhibition*. Published online August 3, 2023. doi:10.58530/2022/2295

[20] Castellanos EA, Du K, Alba D, Hunt P, Koliwad S, Noworolski S. Repeatability and reproducibility of pancreatic proton density fat fraction measurements using manually drawn regions of interest. *Presented at: International Society for Magnetic Resonance in Medicine Annual Meeting;* 2024

[21] Malhotra A, Ayappa I, Ayas N, et al. Metrics of sleep apnea severity: beyond the apnea-hypopnea index. *Sleep*. 2021;44(7):zsab030. doi:10.1093/sleep/zsab030

[22] Isokuortti E, Zhou Y, Peltonen M, et al. Use of HOMA-IR to diagnose non-alcoholic fatty liver disease: a population-based and inter-laboratory study. *Diabetologia*. 2017;60(10):1873-1882. doi:10.1007/s00125-017-4340-1

[23] Hany M, Abouelnasr AA, Abdelkhalek MH, et al. Effects of obstructive sleep apnea on non-alcoholic fatty liver disease in patients with obesity: a systematic review. *Int J Obes (Lond)*. 2023;47(12):1200-1213. doi:10.1038/s41366-023-01378-2

[24] Bonsignore MR, McNicholas WT, Montserrat JM, Eckel J. Adipose tissue in obesity and obstructive sleep apnoea. *Eur Respir J*. 2012;39(3):746-767. doi:10.1183/09031936.00047010

[25] Mirrakhimov AE. Nonalcoholic fatty pancreatic disease and cardio-metabolic risk: is there is a place for obstructive sleep apnea?. *Cardiovasc Diabetol*. 2014;13:29. Published 2014 Jan 30. doi:10.1186/1475-2840-13-29

[26] Rodge GA, Goenka MK, Goenka U, Afzalpurkar S, Shah BB. Quantification of Liver Fat by MRI-PDFF Imaging in Patients with Suspected Non-alcoholic Fatty Liver Disease and Its Correlation with Metabolic Syndrome, Liver Function Test and Ultrasonography. *J Clin Exp Hepatol*. 2021;11(5):586-591. doi:10.1016/j.jceh.2020.11.004

[27] McAnulty RJ. Methods for measuring hydroxyproline and estimating in vivo rates of collagen synthesis and degradation. *Methods Mol Med*. 2005;117:189-207. doi:10.1385/1-59259-940-0:189

[28] Alba DL, Farooq JA, Lin MYC, Schafer AL, Shepherd J, Koliwad SK. Subcutaneous Fat Fibrosis Links Obesity to Insulin Resistance in Chinese Americans. *J Clin Endocrinol Metab*. 2018;103(9):3194-3204. doi:10.1210/jc.2017-02301

[29] Gliniak CM, Pedersen L, Scherer PE. Adipose tissue fibrosis: the unwanted houseguest invited by obesity. *J Endocrinol*. 2023;259(3):e230180. Published 2023 Oct 19. doi:10.1530/JOE-23-0180

[30] Kim Y, Chang Y, Cho YK, Ahn J, Shin H, Ryu S. Metabolically healthy versus unhealthy obesity and risk of fibrosis progression in non-alcoholic fatty liver disease. *Liver Int*. 2019;39(10):1884-1894. doi:10.1111/liv.14184

[31] Guess J, Beltran TH, Choi YS. Prediction of Metabolic Syndrome in U.S. Adults Using Homeostasis Model Assessment-Insulin Resistance. *Metab Syndr Relat Disord*. 2023;21(3):156-162. doi:10.1089/met.2022.0097

Publishing Agreement

It is the policy of the University to encourage open access and broad distribution of all theses, dissertations, and manuscripts. The Graduate Division will facilitate the distribution of UCSF theses, dissertations, and manuscripts to the UCSF Library for open access and distribution. UCSF will make such theses, dissertations, and manuscripts accessible to the public and will take reasonable steps to preserve these works in perpetuity.

I hereby grant the non-exclusive, perpetual right to The Regents of the University of California to reproduce, publicly display, distribute, preserve, and publish copies of my thesis, dissertation, or manuscript in any form or media, now existing or later derived, including access online for teaching, research, and public service purposes.

DocuSigned by:
Siddhartharaja Anbu Rajan
C6B2FD18AC70452...
Author Signature

8/29/2024
Date